JOURNAL OF MATERIALS SCIENCE 26 (1991) 5004–5012

Analysis of the microstructure obtained by using unidirectional solidification, tungsten inert gas weld and laser surface melt traversing techniques in Al–Mn alloys

J. A. JUAREZ-ISLAS
Institute of Physics, Cuernavaca Laboratory, P.O. Box 139-B, C.P. 62191, Cuernavaca, Morelos, Mexico

A major challenge to solidification theory over nearly three decades has been the understanding, prediction and control of rapidly solidified microstructures. The present paper reports results of systematic and controlled conditions of rapid solidification in Al–Mn alloys, which involved measurement of undercooling, solute concentration and cell spacing for solidification front velocities, which were increased progressively, to the level needed for partitionless solidification into a microsegregation-free solid which, in principle, can be crystalline, quasicrystalline or amorphous. Comparison of the measurements with predictions of theoretical modelling give an encouraging level of agreement.

Nomenclature

A	constant $= \pi^2\Gamma/P^2D^2$
A'	constant $= k(\mathrm{ab})^{1/2}$
B	constant $= mC_o p\xi_c/D[1 - pI_v(P)]$
B′	constant
C	$= G(\mathrm{K\,m^{-1}})$
C_{EU}	eutectic composition (at %, wt %)
C_o	alloy concentration (at %, wt %)
C_L^*	tip concentration in liquid (at %, wt %)
C_S^*	tip concentration in solid (at %, wt %)
D	diffusion coefficient in liquid ($\mathrm{m^2\,s^{-1}}$)
G	temperature gradient ($\mathrm{K\,m^{-1}}$)
$I_v(P)$	Ivantsov function ($P\exp(P)E_1(P)$)
P	solute Péclet number $= V_sR/2D$
R	tip radius (m)
T_{EU}	eutectic temperature (K)
T_F	melting point of pure substance (K)
T_G	arrest growth temperature (K)
T_L	liquidus temperature (K)
V_{ab}	absolute stability velocity ($\mathrm{m\,s^{-1}}$)
V_s	solidification front velocity ($\mathrm{m\,s^{-1}}$)
a	material constant
b	material constant
k	distribution coefficient (C_S/C_L)
k	constant
m	liquidus slope (K/at %, K/wt %)
n	exponent
p	complementary distribution coefficient $(1 - k)$
Γ	Gibbs–Thomson coefficient ($\sigma/\Delta s_f$) (Km)
Δs_f	entropy of fusion per mole ($\mathrm{J\,mol^{-1}\,K^{-1}}$)
ΔT_o	liquidus–solidus range at $C_o(T_s - T_L)$ (K)
λ_1	cell spacing (m)
σ	solid/liquid interface energy
π	$= 3.1416$
ξ_c	constant $= 1 - (2k/[1 + (2\pi/P)^2]^{1/2} - 1 + 2k)$

1. Introduction

Solid solubility extension of equilibrium crystalline phases is one of the major constitutional effects of rapid solidification of alloy melts. Thermodynamic conditions for its occurrence, as well as the kinetic considerations affecting the formation of an extended solid solution from a melt of particular alloy composition (i.e. morphological stability and solute trapping) have been discussed in the literature [1]. Advances have also been made recently in modelling the growth of dendrites in the range of velocity approaching that for absolute stability [2–6]. Conditions for microsegregation-free solidification of Ag–Cu alloys by electron-beam surface traversing [7] and measurements of growth temperature, solute concentration and cell spacing of Al–Mn extended solid solutions formed at a sufficiently highly velocity [8–10] showed encouraging agreement with predictions. The present purpose is to summarize here the results obtained for Al–Mn alloys by using the Bridgman unidirectional solidification (UDS), tungsten inert gas (TIG) weld traversing and laser surface melt (LSM) traversing techniques in terms of the formation of α-Al solid solution, coupled eutectic growth and cell spacing.

The experimental procedure has been reported previously [8, 9].

2. Results and discussion

Fig. 1 shows zones of dominant growth structure as a function of solidification front velocity, V_s, and alloy concentration, C_o, for aluminium-rich Al–Mn alloys. The growth velocities in the range 0.1–2 $\mathrm{mm\,s^{-1}}$ are for the Bridgman UDS technique [8]. The results for 2.5–24 $\mathrm{mm\,s^{-1}}$ are for TIG weld while those for

0022–2461/91 $03.00 + .12

21–290 mm s^{-1} are from LSM traversing [10]. Fig. 2a–e shows representative solidification microstructures for alloys and conditions studied.

2.1. Formation of α-Al solid solution

Table I shows a summary of measurements and predictions for growth of unextended (1.3 wt % Mn) and

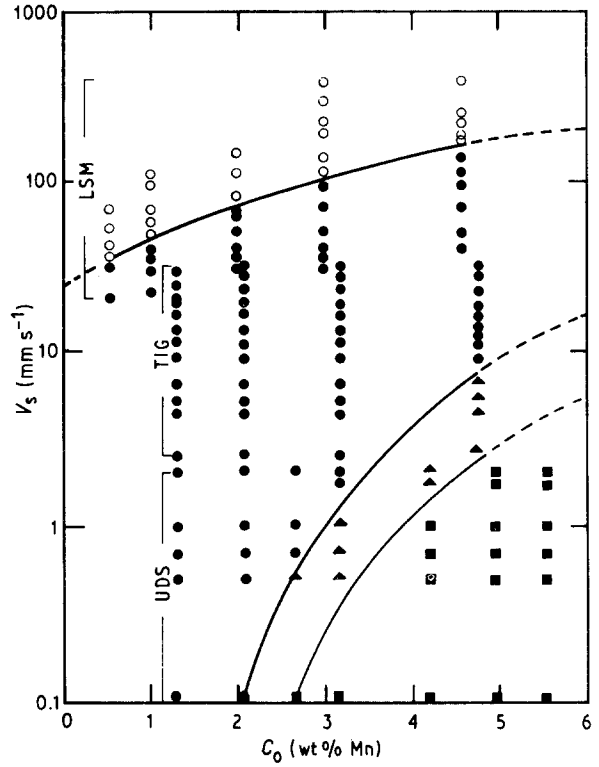

Figure 1 Solidification microstructure as a function of solidification front velocity, V_s, and alloy concentration, C_o, for aluminium-rich Al–Mn alloys, for Bridgman UDS, TIG weld and LSM traversing. (■) Presence of primary Al_6Mn needles, (▲) full eutectic microstructure, (●) primary dendrite cellular α-Al solid solution, (○) microsegregation-free α-Al solid solution.

extended α-Al solid solutions for the UDS and TIG weld experiments (the values employed for the material constraints are given in the Appendix).

Predictions are for the model of Kurz *et al.* [5] for the problem of constrained cellular or dendritic growth at high growth velocity. Their model is an extension of that of Kurz and Fisher [2] but using Ivantsov's solution for the transport problem [11]. In this case, tip concentration $C_s^*(= kC_L^*)$ in the melt and tip temperature, T^*, are given by

$$C_L^* = C_o/[1 - pI_v(P)] \quad (1)$$

and

$$T^* = T_F + mC_L^* - 2\Gamma/R \quad (2)$$

The unknowns P and R are given by solution of

$$V_s^2 A + V_s B + C = 0 \quad (3)$$

Equation 3 was solved numerically with the simplification that $G = 0$ at high V_s to give $P(= RV_s/2D)$ for values of C_o and V_s used in the experiments, so allowing predictions of C_s^* and T^* for comparison with the experimental values.

Fig. 3 shows α-Al dendrite tip undercooling, T^*, as a function of V_s for Al–1.3 and 2.11 wt % Mn alloys for the UDS results. Predictions are in good agreement with the measurements, as are the corresponding ones for the tip concentration C_s^* (for the UDS and TIG weld results), as is shown in Fig. 4. The somewhat higher measured value of tip concentration for the UDS experiments could reflect a contribution from back-diffusion of the solute in the solidified solid [12] which is not taken into account by the model. Manganese content, C_s^*, as a function of growth rate for TIG weld experiments shows a small increase in manganese content in solid solution with increasing growth rate (as V_s approaches the value of V_{ab} the agreement with prediction is excellent).

The amount of manganese (wt %) retained in solid solution for the LSM traversing experiments is shown in Table II for both cellular and microsegregation-free structures. The data show that this retention was uniform and, within experimental limits, at the composition of the parent melt.

The electron microscope microanalysis of manganese content as a function of V_s confirm that the extended solid solutions of manganese in α-Al, containing up to 4.84 wt % Mn, were produced by the TIG weld and LSM traversing experiment conditions.

Interpretation of the observed dependences of the dendrite tip undercooling, T^* (UDS results), and of the manganese content, C_s^* (UDS and TIG weld results), as a function of V_s and C_o shown in Figs 3 and 4, respectively, involves recourse to the theory of dendrite growth. These dependences are in good agreement with predictions.

As is shown in Fig. 1, results from the Bridgman UDS, TIG weld and LSM traversing all showed that the cellular α-Al solid solution could be obtained in Al–Mn alloys with manganese contents beyond that (C_{EU} = 2.0 wt % Mn [13]) in the eutectic composition. Even this was eliminated at solidification front velocities (achieved in the LSM traversing experiments) above 36, 58, 80, 106 and 176 mm s^{-1} for Al–0.5, 1, 2, 3 and 4.6 wt % Mn, respectively, producing a cell-free microstructure. Earlier, Schaefer *et al.* [14] carried out electron-beam melt traversing experiments on Al–0.1, 0.25 and 1.0 wt % Mn alloys, using scan speeds in the range 10^{-2}–1 m s^{-1} and reported a cell-free structure for the first two alloys. However, the transition velocity from a cellular to a cell-free structure was not specified. Microsegregation-free microstructures have also been reported [14] for Ag–Cu alloys at solidification front velocities of 150 mm s^{-1} (Ag–1.0 wt % Cu) and 600 mm s^{-1} (Ag–5 wt % Cu). Such velocities, for both Ag–Cu and Al–Mn, are well below those of about 5 m s^{-1} normally associated in dilute alloys with solute trapping [1]. However, microsegregation-free microstructures become possible at lower velocity than this because of the incidence of absolute interfacial stability, which is predicted [15] for an initial alloying element concentration, C_o, if the growth rate, V_{ab}, exceeds a critical

TABLE I Summary of measurements and predictions for growth of unextended (1.3 wt % Mn) and extended α-Al solid solutions for the UDS and TIG experiments

Alloy composition (wt %)		Growth velocity, V_s (mm s^{-1})	Measurements				Predictions		
			Arrest (growth) temperature, T_G (°C)	Growth undercooling, ΔT (K)	Cell tip concentration, C_s^* (wt % Mn)	Cell spacing, λ (μm)	Growth undercooling, ΔT (K)	Cell tip concentration, C_s^* (wt % Mn)	Cell spacing, λ (μm)
1.30	UDS	0.102	658.90 ± 0.10	0.12	1.22 ± 0.02	33.5 ± 1.90	0.14	1.04	47.7
		0.514	658.82 ± 0.12	0.20	1.24 ± 0.02	19.0 ± 0.70	0.24	1.10	31.8
		0.715	658.75 ± 0.15	0.27	1.24 ± 0.03	16.0 ± 0.20	0.22	1.11	29.3
		1.010	658.72 ± 0.12	0.30	1.25 ± 0.03	12.6 ± 0.50	0.23	1.13	26.9
		2.000			1.30 ± 0.03	8.1 ± 0.10		1.16	22.6
	TIG	4.400	–	–	1.25 ± 0.03	6.0 ± 0.20	–	1.218	18.6
		4.900	–	–	1.26 ± 0.03	5.5 ± 0.15	–	1.222	18.1
		7.900	–	–	1.265 ± 0.02	4.7 ± 0.20	–	1.254	14.9
		11.100	–	–	1.27 ± 0.02	4.2 ± 0.15	–	1.258	14.7
		12.000	–	–	1.272 ± 0.04	4.1 ± 0.15	–	1.272	14.4
		15.700	–	–	1.28 ± 0.03	3.6 ± 0.14	–	1.294	13.5
		19.000	–	–	1.286 ± 0.03	3.2 ± 0.18	–	1.296	12.9
		25.500	–	–	1.29 ± 0.01	2.9 ± 0.11	–	1.297	12.0
		27.700	–	–	1.294 ± 0.03	2.8 ± 0.11	–	1.300	11.7
2.11	UDS	0.102	658.28 ± 0.12	0.20	2.01 ± 0.05	16.1 ± 0.05	0.27	1.66	53.8
		0.514	658.10 ± 0.07	0.38	2.05 ± 0.03	14.4 ± 0.04	0.39	1.75	35.9
		0.715	658.06 ± 0.10	0.42	2.06 ± 0.03	12.2 ± 0.4	0.42	1.77	33.1
		1.010	657.96 ± 0.15	0.52	2.07 ± 0.09	9.9 ± 0.2	0.45	1.80	30.3
		2.000	–	–	2.10 ± 0.03	8.4 ± 0.1	–	1.85	25.5
	TIG	4.300	–	–	2.051 ± 0.024	5.0 ± 0.2	–	1.945	21.1
		9.000	–	–	2.060 ± 0.030	4.6 ± 0.7	–	1.981	17.5
		9.500	–	–	2.067 ± 0.028	4.4 ± 0.5	–	2.000	17.3
		11.800	–	–	2.075 ± 0.026	3.8 ± 0.10	–	2.011	16.4
		16.100	–	–	2.083 ± 0.031	2.7 ± 0.11	–	2.018	15.1
		22.000	–	–	2.092 ± 0.015	2.5 ± 0.11	–	2.062	14.0
		24.000	–	–	2.104 ± 0.035	2.3 ± 0.20	–	2.070	13.7
2.68	UDS	0.715	–	–	2.58 ± 0.50	10.8 ± 0.20	–	2.23	35.1
		1.010	–	–	2.62 ± 0.08	8.7 ± 0.1	–	2.26	32.2
		2.000	–	–	2.66 ± 0.09	5.5 ± 0.2	–	2.32	27.1
3.18	UDS	1.720	–	–	3.08 ± 0.03	6.7 ± 0.1	–	2.72	29.3
		2.000	–	–	3.10 ± 0.02	4.9 ± 0.1	–	2.74	28.2
	TIG	4.300	–	–	3.085 ± 0.021	4.6 ± 0.16	–	2.900	23.3
		9.000	–	–	3.090 ± 0.021	4.2 ± 0.20	–	2.982	19.4
		9.500	–	–	3.096 ± 0.017	4.1 ± 0.15	–	3.000	19.1
		11.800	–	–	3.101 ± 0.020	3.2 ± 0.10	–	3.036	18.1
		16.100	–	–	3.123 ± 0.021	2.5 ± 0.10	–	3.072	16.7
		22.000	–	–	3.151 ± 0.056	2.4 ± 0.12	–	3.112	15.5
		24.000	–	–	3.157 ± 0.036	2.25 ± 0.11	–	3.109	15.2
4.84	TIG	9.500	–	–	4.785 ± 0.010	2.1 ± 0.0	–	4.380	21.3
		11.800	–	–	4.790 ± 0.018	1.9 ± 0.16	–	4.418	20.2
		16.100	–	–	4.797 ± 0.025	1.7 ± 0.18	–	4.450	18.7
		22.000	–	–	4.813 ± 0.030	1.37 ± 0.20	–	4.491	17.2
		24.000	–	–	4.825 ± 0052	1.30 ± 0.05	–	4.527	16.9

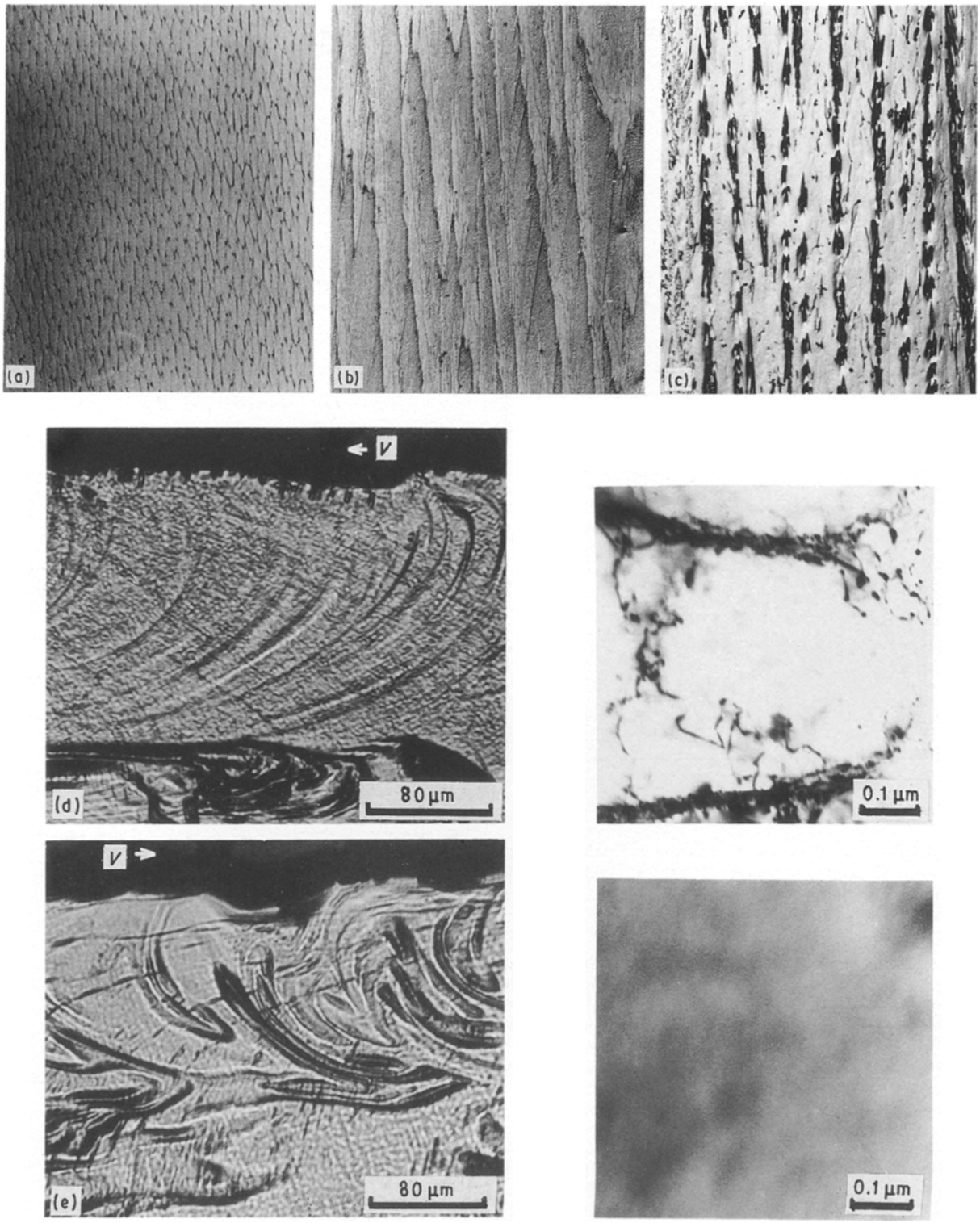

Figure 2 Representative solidification microstructures for alloys and conditions studied. (a) Extended α-Al solid solution in Al–2.11 wt % Mn at 0.514 mm s^{-1}, × 105. (b) Full eutectic microstructure in Al–3.18 wt % Mn at 0.714 mm s^{-1}, × 100. (c) Primary Al_6Mn in α-Al solid solution in Al–4.2 wt % Mn a 0.101 mm s^{-1}, × 100. (d) Longitudinal section of a LSM traversing Al–2.0 wt % Mn alloy scanned at 250 mm s^{-1} (left). Transmission electron micrograph of the cellular microstructure observed in this alloy at that scan velocity. (e) Longitudinal section of a LSM traversing Al–3.0 wt % Mn alloy scanned at 400 mm s^{-1} (left). Transmission electron micrograph of the microsegregation-free structure observed in this alloy at that scan velocity.

value given by

$$V_{ab} = mD(1 - k)C_o/k^2\Gamma \quad (4)$$

The conditions for absolute stability appear to have been met in the LSM traversing experiments. Table III summarizes the values of V_{ab} predicted (for $k = 0.5$ and 0.7) according to Equation 4 for comparison with values of V_{obs} found to be required for segregation-free solidification of the Al–0.5, 1.0, 2.0, 3.0 and 4.6 wt % Mn alloys. This table shows that the observed velocities for segregation-free solidification are factors of 6, 5 and 4 (for $k = 0.7$), higher than predicted for the absolute stability criterion for Al–0.5, 1.0 and 2–4.6 wt % Mn, respectively. This can be considered to represent reasonable agreement in view of possible uncertainties in applicable values of k, m and D. For

instance, a reduction in k from 0.7 to 0.5 will virtually eliminate these discrepancies between observed and predicted V_{ab}.

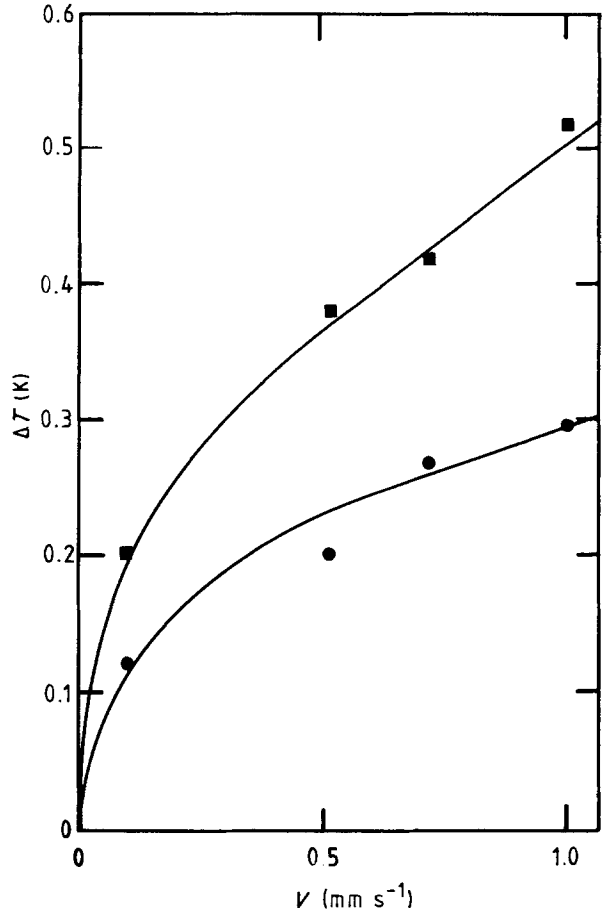

Figure 3 Growth undercooling as a function of V_s for unextended (●, 1.3 wt % Mn) and extended (■, 2.11 wt % Mn) α-Al solid solutions. Points represent measurements while lines are predictions, see text.

TABLE II Measurements of cell tip concentration, C_s^*, for microsegregation-free and elongated cellular structures for the laser-surface-melted specimens

Alloy composition (wt %)	Mn retained in cellular solid solution at growth rates in the range 30–40 mm s^{-1} (wt %)	Mn retained in the microsegregation-free microstructure at a growth rate of 112 mm s^{-1} (wt %)
Al–0.5Mn	0.490 ± 0.005	0.50 ± 0.009
Al–1.0Mn	1.052 ± 0.001	1.00 + 0.011
Al–2.0Mn	1.984 ± 0.004	1.99 ± 0.017
Al–3.0Mn	2.953 ± 0.011	3.00 ± 0.010
Al–4.6Mn	4.572 ± 0.007	4.60 ± 0.030

2.2. Coupled eutectic growth

Growth temperature, T_G, for the eutectic is predicted [16] and found experimentally [17] to conform with

$$T_{EU} - T_G = A'V_s^{1/2} \quad (5)$$

The corresponding relation for dendrite growth is more complex but can be represented to a good approximation by [18]

$$T_L - T_G = GD/V_s + B'V_s^n \quad (6)$$

The limiting condition for single-phase (e.g. α-Al solid solution) growth at the same temperature as a eutectic is obtained by solving Equations 5 and 6 simultaneously to give the limiting growth velocity as the solution of

$$T_L - T_{EU} = GD/V_s + B'V_s^n - A'V_s^{1/2} \quad (7)$$

The constant A' for eutectic growth is predicted to be equal to $K(ab)^{1/2}$ where a and b are materials constants and K is theoretically equal to 2. Table IV reports an analysis of measurements for the Al–Al_6Mn eutectic containing 3.18 wt % Mn, giving A' as 0.0602 K s$^{1/2}$ μm$^{-1/2}$. The correspondng predicted values (see Table V) of $a = 0.269$ μm K and

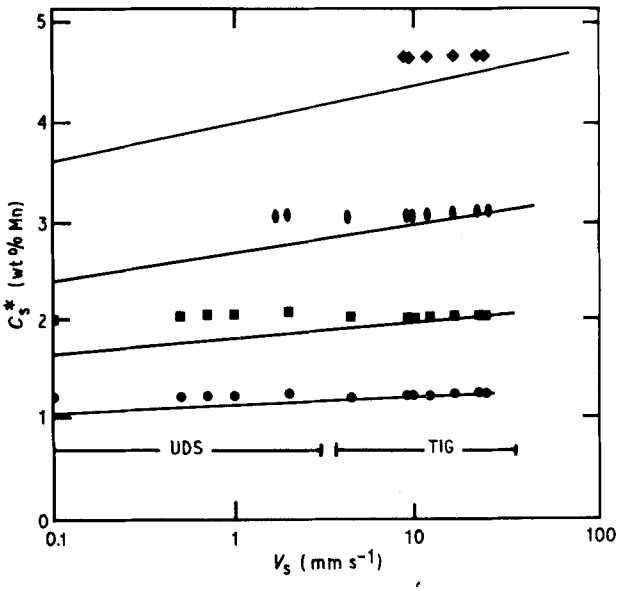

Figure 4 (●, ■, ⬮, ◆) Measurements and (——) predictions of the manganese concentration, C_s^*, determined by electron microanalysis as a function of growth velocity, V_s, and alloy concentration, C_o, for the cellular α-Al solid solutions obtained by Bridgman UDS and TIG weld traversing. (●) Al–1.30 wt % Mn, (■) Al–2.11 wt % Mn, (⬮) Al–3.18 wt % Mn, (◆) Al–4.80 wt % Mn.

TABLE III Predicted velocity, V_{ab}, for absolute stability in the solidification of Al–Mn alloys compared with observed velocity, V_{obs}, required for segregation-free solidification

Alloy composition (wt %)	V_{ab_1} (for $k = 0.7$) (mm s^{-1})	V_{ab_2} (for $k = 0.5$) (mm s^{-1})	V_{obs} (mm s^{-1})	V_{obs}/V_{ab_1}	V_{obs}/V_{ab_2}
Al–0.5Mn	5.3	16.6	36	6.8	2.1
Al–1.0Mn	10.2	33.3	58	5.7	1.7
Al–2.0Mn	20.4	66.6	80	3.9	1.2
Al–3.0Mn	30.6	100.0	100	3.2	1.0
Al–4.6Mn	46.9	153.3	176	3.7	1.1

TABLE IV Analysis of measurements for the Al–Al_6Mn eutectic containing 3.18 wt % Mn

Growth velocity, V (mm s^{-1})	Arrest (growth) temperature, T_G (°C)	Growth undercooling, ΔT (K)	Interphase spacing, λ (μm)	$\Delta T/V^{1/2}$ (K $s^{1/2}$ $\mu m^{-1/2}$)	$\lambda V^{1/2}$ ($\mu m^{3/2}$ $s^{-1/2}$)	$\Delta T\lambda$ (K μm)	$\Delta T/V\lambda$ (K s μm^{-2})
0.102	657.8 ± 0.10	0.60	1.75 ± 0.09	0.0595	17.7	1.05	0.003 36
0.514	657.1 ± 0.10	1.35	0.94 ± 0.08	0.0595	21.3	1.26	0.002 79
0.715	656.8 ± 0.09	1.61	0.65 ± 0.07	0.0602	17.3	1.04	0.003 47
1.010	656.5 ± 0.10	1.96	0.49 ± 0.07	0.0617	15.5	0.96	0.003 99

TABLE V Limiting velocities V_α, V_β for growth of primary α-Al and primary Al_6Mn as a function of alloy concentration, C_o, with derived parameters B for dendritic growth of α-Al and Al_6Mn

C_o (wt % Mn)	V_α (mm s^{-1})	V_β (mm s^{-1})	a (μm K)	b (10^{-4} K s μm^{-2})	$A = 5.78(ab)^{1/2}$ (K $s^{1/2}$ $\mu m^{-1/2}$)	B_α (K $s^{1/2}$ $\mu m^{1/2}$)	B_β (K $s^{1/2}$ $\mu m^{1/2}$)
2.11	0.10	–	0.300	2.39	0.0490	0.0408	–
2.68	0.65	0.25	0.293	2.57	0.0591	0.0391	1.410
3.18	1.01	0.51	0.269	4.03	0.0602	0.0293	1.509
4.26	2.00	1.15	0.255	5.55	0.0688	0.0310	1.677
4.84	5.90	1.80	0.254	5.65	0.0690	0.0423	1.606
5.08	7.00	2.00	0.235	6.41	0.0737	0.0461	1.595

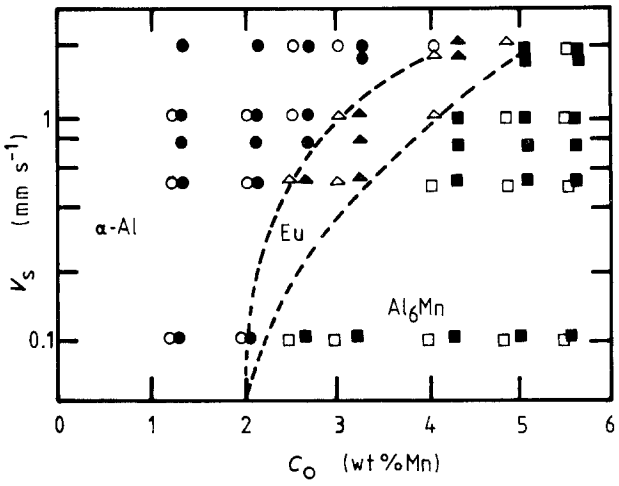

Figure 5 Solidification microstructure as a function of growth velocity, V_s, and alloy concentration, C_o, for aluminium-rich Al–Mn alloys. (□, △, ○) [25]. (□, ■) Primary Al_6Mn, (△, ▲) full eutectic microstructure, (○, ●) α-Al solid solution.

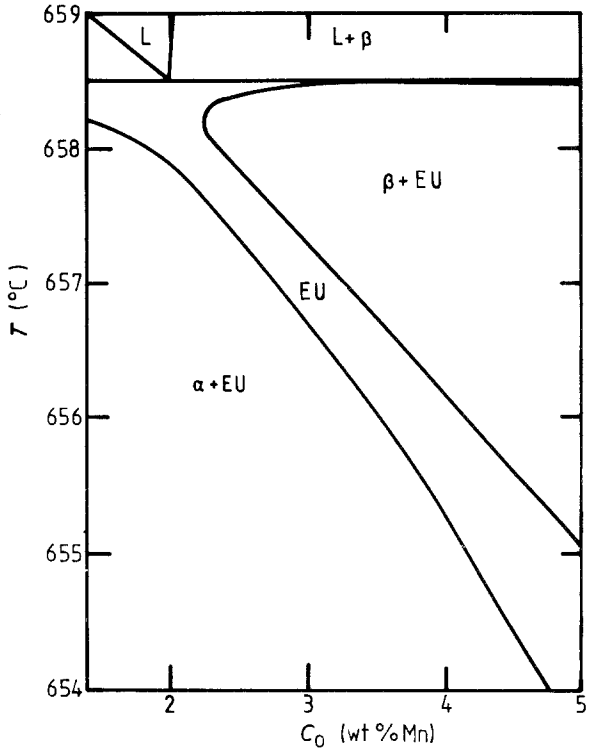

Figure 6 Aluminium-rich Al–Mn phase diagram (from [13]), showing the predicted coupled zone for α-Al–Al_6Mn eutectic growth.

$b = 0.000\,403$ K s μm^{-2} for this composition then give $K = 5.78$ compared with the "theoretical" value of 2. The values B_α and B_β (Table V) of B' as a function of alloy concentration C_o for the extended α-Al solid solution and primary Al_6Mn consistent with the positions of the α-Al/eutectic (EU) and Al_6Mn/EU boundaries shown in Fig. 5 were obtained from Equation 6 by substituting $A' = 5.78(ab)^{1/2}$, T_α (°C) = 660–0.75C_o (wt %), T_β (°C) = 658.5 + 28.87 $(C_o - 2)^{0.18}$ and $T_{EU} = 658.5$ °C. The value of B_α (0.043 ± 0.003 K $s^{1/2}$ $\mu m^{-1/2}$) is two to three times larger than given by the direct measurements of $T_\alpha - T_G$ as a function of V_s reported previously [8] for the alloys containing 1.3 and 2.11 wt % Mn. The value of B_β(1.56 ± 0.11 K $s^{1/2}$ $\mu m^{-1/2}$) is significantly larger than B_α consistent with the larger undercooling expected to be required to sustain growth of a facetted phase of relatively complex crystal structure. These values of B_α and B_β can be employed to derive the growth temperature versus concentration limits for coupled eutectic growth by substituting V_s from Equation 7 into Equation 5 or 6 with $n = 1/2$. The resulting coupled zone is superimposed on the phase diagram in Fig. 6 and on a plot of V_s versus C_o in Fig. 7.

Competitive growth considerations predict that the resulting structure under the given growth conditions is that growing at the highest solidification front velocity for an imposed growth temperature, or at the

highest growth temperature for an imposed solidification front velocity. This situation is shown schematically in Fig. 8, in which the curves of growth temperature against solidification front velocity for the α-Al solid solution, α-Al–Al_6Mn eutectic and Al_6Mn are shown for $G = 10\,K\,mm^{-1}$ together with the experimental points from [8] for an Al–3.18 wt % Mn alloy. These curves are consistent with observations that Al_6Mn will grow at solidification front velocities, $V_s < 500\,\mu m\,s^{-1}$, α-Al–Al_6Mn eutectic in the range $500 < V_s < 1100\,\mu m\,s^{-1}$, and the α-Al solid solution at $V_s > 1100\,\mu m\,s^{-1}$.

2.3. Cell spacing

Fig. 9 shows α-Al cell spacing as a function of solidification front velocity and initial manganese concentration, and it shows that the spacing decreases with increasing growth rate and initial manganese concentration. An apparently stronger dependence of λ_1 on V_s is shown in the figure, than those predicted by the Hunt [19] and the Kurz and Fisher [2] models. For the UDS results, λ_1 at fixed V_s is observed to decrease with increasing manganese concentration while the predicted values do the reverse (see [8]). The predicted dependence stems from an assumed increase in α-Al melting range, ΔT_o, with increasing C_o in the range 1.3–4.84 wt % Mn. If, however, ΔT_o decreases with increasing C_o in this range because of a minimum in the α-Al solidus–liquidus curves at some higher value of C_o, λ_1 is then predicted to decrease with increasing C_o, as observed.

In order to determine whether or not the observed dependences of λ_1 on V_s and C_o at high V_s are better represented by some simple function of the predicted cell tip radius, R, as determined, for example, by the marginal stability considerations applied to the cell tip advancing at high V_s, Kurz *et al.* [5] have shown that a good approximation for R under such conditions of high Péclet number is

$$R = 2\pi(D\Gamma/V_s\Delta T_o)^{1/2} \quad (8)$$

This equation thus predicts that R will decrease parabolically with increase of both V_s and ΔT_o (or C_o). In contrast, the equations of Hunt [19] and Kurz and Fisher [2] for λ_1 give, respectively

$$\lambda_1 = 2.83(k\Delta T_o D\Gamma/V_s)^{1/4} G^{-1/2} \quad (9)$$

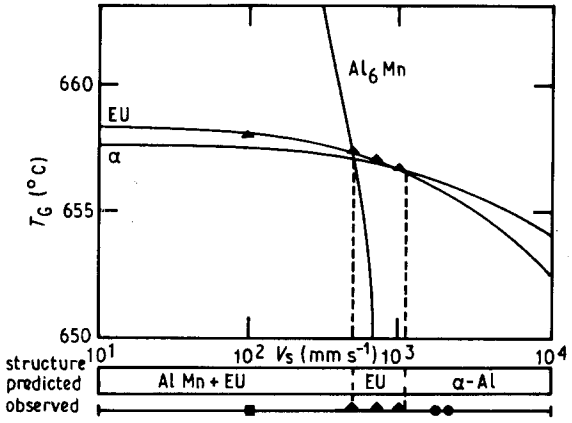

Figure 8 Growth temperature as a function of growth velocity, V_s, in Al–3.18 wt % Mn ($G = 10\,K\,mm^{-1}$) for (●) α-Al solid solution (Eu), eutectic and (Al_6Mn) primary Al_6Mn. (■) Presence of primary Al_6Mn + eutectic, (▲) fully eutectic microstructure, (●) primary α-Al solid solution.

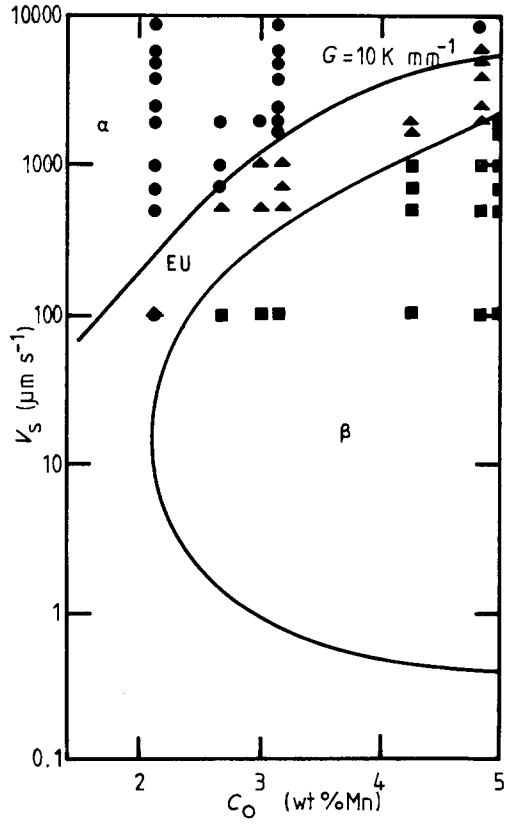

Figure 7 Predicted coupled zone compared with actual solidification microstructure as a function of growth velocity, V_s, and alloy composition, C_o, for aluminium-rich Al–Mn alloys. (■) Primary Al_6Mn, (▲) full eutectic, (●) α-Al solid solution.

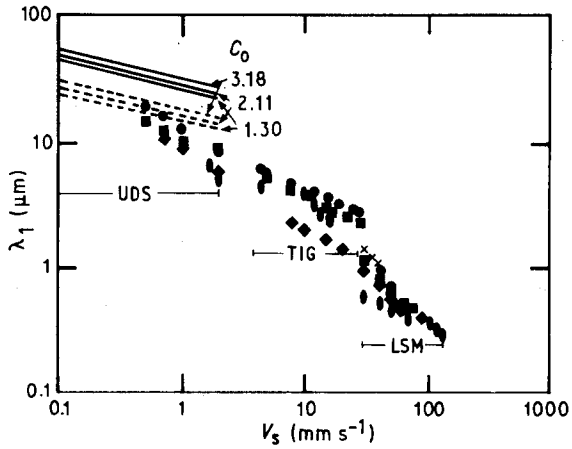

Figure 9 (+ , ●, ■, ◆, ⬮) Measurements and (—— [2], – – – [19]) predictions of the cell spacing, λ_1, as a function of the growth velocity, V_s, and the initial manganese concentration alloy, C_o, for the cellular α-Al solid solutions obtained by Bridgman UDS, TIG weld and LSM traversing. (+) Al–0.5 wt % Mn, (●) Al–1 (LSM)–1.30 (UDS and TIG) wt % Mn, (■) Al–2 (LSM)–2.11 (UDS and TIG) wt % Mn, (◆) Al–2.7 (UDS) wt % Mn, (◆) Al–3 (LSM)–3.18 (UDS and TIG) wt % Mn, (◆) Al–4.8 (TIG) wt % Mn, (⬮) Al–4.6 (LSM) wt % Mn.

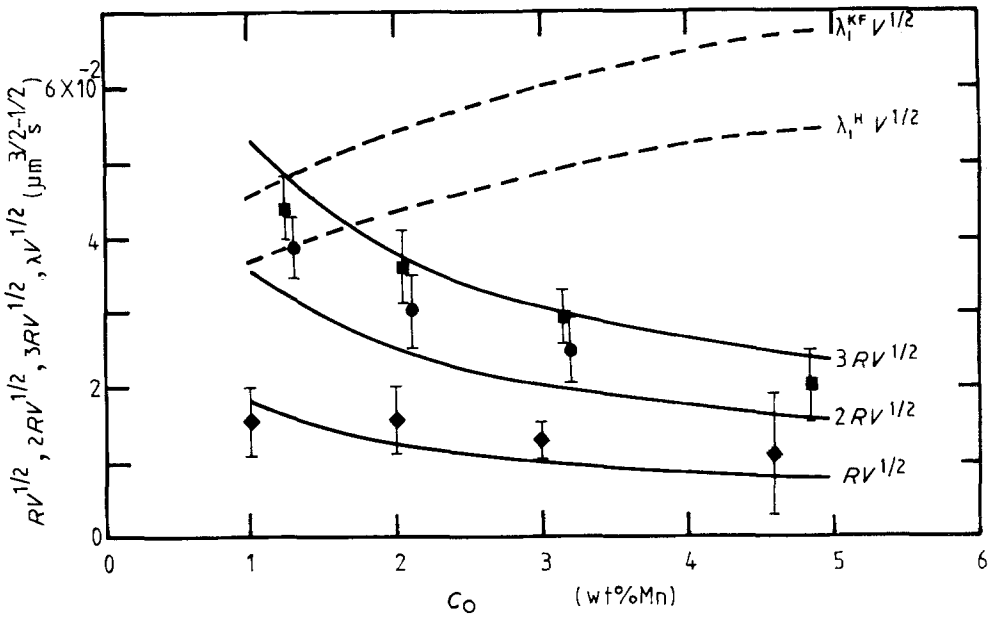

Figure 10 $RV^{1/2}$, $2RV^{1/2}$, $3RV^{1/2}$ and $\lambda V^{1/2}$ plotted gainst C_o together with $\lambda_1^H V^{1/2}$ and $\lambda_1^{KF} V^{1/2}$ according to Equations 9 and 10, respectively. Experimental points are mean vaues, with ranges of scatter shown for the range of V_s studied for each alloy concentration, C_o. (●) UDS, (■) TIG, (◆) LSM.

and

$$\lambda_1 = 4.30(\Delta T_o D\Gamma/kV_s)^{1/4} G^{-1/2} \qquad (10)$$

showing a dependence on temperature gradient, G, that is absent from Equation 8, a weaker dependence on V_s and a predicted increase in λ_1 with increasing ΔT_o or C_o.

Fig. 10 shows a plot of $RV^{1/2}$, $2RV^{1/2}$ and $3RV^{1/2}$ against alloy concentration, C_o, together with the predictions of Equations 9 and 10 for $\lambda_1 V^{1/2}$. The experimental data for λ_1 show excellent agreement with the dependence on C_o predicted by Equation 8 whereas Equations 9 and 10 predict an increase in $\lambda_1 V^{1/2}$ with increasing C_o, which is not observed in this case. While there is the possibility that a minimum in the extended α-Al solidus–liquidus curves at some higher value of C_o, as proposed in [10], could reverse the concentration dependence predicted by Equations 9 and 10 in this concentration range, it still remains to be established whether or not this could be sufficient to match theory with experiment.

3. Conclusions

1. Measurements of growth temperature and of tip concentration on the front velocity, V_s, and initial manganese concentration, C_o, for a terminal solid solution extended by rapid solidification were found to be in good agreement with the predictions of the dendrite growth theory.

2. Segregation-free solidification was obtained at solidification front velocities which increased with increasing manganese concentration. Predicted values of the velocity required for absolute stability of growth of the extended α-Al solid solution are (for $k = 0.7$) four to six times lower than determined experimentally for segregation-free solidification; this may be considered to represent reasonable agreement in view of the uncertainty of the diffusion and phase diagram data.

3. Measurements of growth undercooling as a function of growth velocity (> 0.1 mm s^{-1}) for the α-Al–Al_6Mn eutectic together with measurements of the limiting velocities for growth of primary α-Al and primary Al_6Mn as a function of alloy concentration, have been used to derive values for dendritic growth parameters of α-Al and Al_6Mn, and the corresponding growth temperature versus concentration coupled-zone boundaries for the α-Al–Al_6Mn system.

4. Cell spacing decreased with increasing growth rate, in agreement with predictions. Observed values decrease with increase in manganese level which would require a minimum in the α-Al solidus–liquidus curves at some higher value of C_o to be consistent with predictions.

Appendix. Values employed for the material constraints

$D = 2.4 \times 10^{-9}$ m^2 s^{-1} (mean of 2.1×10^{-9} from Takahashi *et al.* [20] and 2.7×10^{-9} m^2 s^{-1} from Sugiyama *et al.* [21]).
$G = 10$ K/mm for the UDS experiments [22].
$k = 0.7$ [13].
$m = 0.75$ K/wt % [13].
$\Gamma = 1.08 \times 10^{-7}$ Km (σ from [23] and ΔS_f from [24]).

References

1. W. J. BOETTINGER, S. R. CORIEL and R. F. SEKERKA, *Mater. Sci. Engng* **65** (1984) 27.
2. W. KURZ and D. J. FISHER, *Acta Metall.* **29** (1981) 11.
3. V. LAXMANAN, *ibid.* **33** (1985) 1023.
4. *Idem., ibid.* **33** (1985) 1037.
5. W. KURZ, B. GIOVANOLA and R. TRIVEDI, *ibid.* **34** (1986) 823.
6. R. TRIVEDI and W. KURZ, *ibid.* **34** (1986) 1663.

7. W. J. BOETTINGER, D. SHECHTMAN, R. J. SCHAEFER and F. S. BIANCANIELLO, *Metall. Trans.* **15A** (1984) 55.
8. J. A. JUAREZ-ISLAS and H. JONES, *Acta Metall.* **35** (1987) 499.
9. *Idem., Inst. Metals* **421** (1988) 492.
10. J. A. JUAREZ-ISLAS, H. JONES and W. KURZ, *Mater. Sci. Engng* **98** (1988) 201.
11. H. ESAKA and W. KURZ, *J. Crystal Growth* **69** (1984) 362.
12. H. D. BRODY and M. C. FLEMINGS, *Metal Trans.* **12A** (1981) 965.
13. M. HANSEN and K. ANDERKO (eds), "Constitution of Binary Alloys" (McGraw-Hill, New York, 1958).
14. R. J. SCHAEFER, S. R. CORIELL, R. MEHRABIAN, C. FENIMORE and F. S. BIANCANIELLO, in "Rapidly Solidified Amorphous and Crystalline Alloys", edited by B. H. Kear, B. C. Giessen and M. Cohen, Materials Research Society Symposium Proceedings, Vol. 8 (Elsevier, Amsterdam, 1982) p. 79.
15. W. W. MULLINS, A. J. McALISTER, R. J. SCHJAEFER, L. A. BENDERSKY, F. S. BIANCANIELLO and D. L. MOFFAT, *Metall. Trans.* **18A** (1987) 385.
16. K. A. JACKSON and J. D. HUNT, *Trans. Met. Soc. AIME* **236** (1966) 1129.
17. W. KURZ and D. J. FISHER, *Int. Met. Rev.* **24** (1979) 177.
18. W. KURZ, *Z. Metallkde.* **69** (1978) 433.
19. J. D. HUNT, in "Proceedings of the Conference on Solidification and Casting of Metals", Sheffield, July 1977 (Metals Society, London, 1979) pp. 3–9.
20. T. TAKAHASHI, A. KAMIO and NGUYEN AN TRUNG, *J. Crystal Growth* **24/25** (1974) 477.
21. M. SUGIYAMA, T. UMEDA and H. KATO, *J. Jpn Inst. Light Metals* **24** (1974) 263.
22. J. A. JUAREZ-ISLAS, PhD thesis, Sheffield University (1986).
23. R. H. EWING, *Phil. Mag.* **25** (1972) 779.
24. C. J. SMITHELLS and E. A. BRANDES (eds), "Metals Reference Book", 5th Edn (Butterworths, London, 1976).
25. J. A. EADY *et al., J. Aust. Inst. Metals* **28** (1975) 23.

Received 16 July 1990
and accepted 6 February 1991